Biochimica et Biophysica Acta 1847 (2015) 276–285

Contents lists available at ScienceDirect

Biochimica et Biophysica Acta

journal homepage: www.elsevier.com/locate/bbabio

Assembly of oxygen-evolving Photosystem II efficiently occurs with the apo-Cytb_{559} but the holo-Cytb_{559} accelerates the recovery of a functional enzyme upon photoinhibition

Miwa Sugiura [a,b,c,*], Makoto Nakamura [b], Kazumi Koyama [a], Alain Boussac [d,**]

[a] Proteo-Science Research Center, Ehime University, Bunkyo-cho, Matsuyama, Ehime 790-8577, Japan
[b] Department of Chemistry, Graduate School of Science and Technology, Ehime University, Bunkyo-cho, Matsuyama, Ehime 790-8577, Japan
[c] PRESTO, Japan Science and Technology Agency (JST), 4-1-8, Honcho, Kawauchi, Saitama 332-0012, Japan
[d] iBiTec-S, CNRS UMR 8221, CEA Saclay, 91191 Gif-sur-Yvette, France

ARTICLE INFO

Article history:
Received 14 October 2014
Received in revised form 17 November 2014
Accepted 26 November 2014
Available online 3 December 2014

Keywords:
Photosystem II
Cytb_{559}
Haem axial ligands
Photoinhibition

ABSTRACT

Cytb_{559} in Photosystem II is a heterodimeric b-type cytochrome. The subunits, PsbE and PsbF, consist each in a membrane α-helix. Roles for Cytb_{559} remain elusive. In *Thermosynechococcus elongatus*, taking advantage of the robustness of the PSII variant with PsbA3 as the D1 subunit (WT*3), 4 mutants were designed hoping to get mutants nevertheless the obligatory phototrophy of this cyanobacterium. In two of them, an axial histidine ligand of the haem-iron was substituted for either a methionine, PsbE/H23M, which could be potentially a ligand or for an alanine, PsbE/H23A, which cannot. In the other mutants, PsbE/Y19F and PsbE/T26P, the environment around PsbE/H23 was expected to be modified. From EPR, MALDI-TOF and O_2 evolution activity measurements, the following results were obtained: Whereas the PsbE/H23M and PsbE/H23A mutants assemble only an apo-Cytb_{559} the steady-state level of active PSII was comparable to that in WT*3. The lack of the haem or, in PsbE/T26P, conversion of the high-potential into a lower potential form, slowed-down the recovery rate of the O_2 activity after high-light illumination but did not affect the photoinhibition rate. This resulted in the following order for the steady-state level of active PSII centers under high-light conditions: PsbE/H23M ≈ PsbE/H23A << PsbE/Y19F ≤ PsbE/T26P ≤ WT*3. These data show i) that the haem has no structural role provided that PsbE and PsbF are present, ii) a lack of correlation between the rate of photoinhibition and the E_m of the haem and iii) that the holo-Cytb_{559} favors the recovery of a functional enzyme upon photoinhibition.

The light-driven oxidation of water in Photosystem II (PSII) is the first step in the photosynthetic production of most of biomass, fossil fuels and O_2 on Earth. PSII in cyanobacteria is made up of 17 membrane protein subunits and 3 extrinsic proteins. Although the PsbY subunit was not detected in [1] it was seen in [2,3]. Altogether these 20 subunits bear 35 chlorophylls, 2 pheophytins (Phe), 2 haems, 1 non-haem iron, 2 plastoquinones (Q_A and Q_B), a Mn_4CaO_5 cluster, 2 Cl^-, 12 carotenoids and 25 lipids [1]. The excitation resulting from the absorption of a photon is transferred to the photochemical trap that undergoes charge separation. The positive charge is then stabilized on P_{680} which is composed of four chlorophyll *a* molecules, P_{D1}/P_{D2} and Chl_{D1}/Chl_{D2}, and two pheophytin *a* molecules, Phe_{D1}/Phe_{D2}. Then, $P_{680}^{+\bullet}$ oxidizes Tyr_Z, the Tyr161 of the D1 polypeptide, which in turn oxidizes the Mn_4CaO_5 cluster. On the electron acceptor side, the electron is transferred to the primary quinone electron acceptor, Q_A, and then to Q_B, a two-electron and two-proton acceptor, *e.g.* [4–6]. The Mn_4CaO_5 cluster accumulates oxidizing equivalents and acts as the catalytic site for water oxidation. The enzyme cycles sequentially through five redox states denoted S_n where *n* stands for the number of stored oxidizing equivalents. Upon formation of the S_4 state two molecules of water are rapidly oxidized, the S_0 state is regenerated and O_2 is released, *e.g.* [5–12].

Two hemoproteins associate with PSII complex [1]. One is the extrinsic Cytc_{550} found in red algae and cyanobacteria, reviewed in [13], the second is Cytb_{559} that is present in all photosynthetic species and is located in the membrane at the periphery of PSII [1]. Cytb_{559} is a heterodimer with two subunits, α and β (encoded by the *psbE* and *psbF* genes), of ≈ 9 kDa and ≈ 5 kDa, respectively, both having an α-helix spanning

Abbreviations: PSII, Photosystem II; Chl, chlorophyll; MES, 2–(N–morpholino) ethanesulfonic acid; P_{680}, chlorophyll dimer acting as the electron donor; Q_A, primary quinone acceptor; Q_B, secondary quinone acceptor; Cm, chloramphenicol; Sm, streptomycin; Sp, spectinomycin; 43H, *T. elongatus* strain with a His–tag on the C terminus of CP43; PQ, plastoquinone 9; WT*3, cells containing only the *psbA*$_3$ gene; $Pheo_{D1}$, pheophytin; P_{D1} and P_{D2}, Chl monomer of P_{680} on the D1 or D2 side, respectively; Cyt, cytochrome; PPBQ, phenyl *p*–benzoquinone; DCBQ, 2,6-dichloro-*p*-benzoquinone; β–DM, *n*–dodecyl–β–maltoside; MALDI-TOF, matrix-assisted laser desorption/ionization-time of flight; HP, IP, LP, forms are high-potential, intermediate-potential and low-potential forms of Cytb_{559}

* Correspondence to: M. Sugiura, Proteo-Science Research Center, Ehime University, Bunkyo-cho, Matsuyama, Ehime, 790-8577, Japan.
** Corresponding author.
E-mail addresses: miwa.sugiura@ehime-u.ac.jp (M. Sugiura), alain.boussac@cea.fr (A. Boussac).

http://dx.doi.org/10.1016/j.bbabio.2014.11.009
0005-2728/

the thylakoid membrane (Fig. 1A). In the thermophilic cyanobacterium *Thermosynechococcus elongatus*, the two axial ligands of the haem iron are PsbE/His23 and PsbF/His24.

The precise role(s) for these two cytochromes is(are) still today not completely understood despite considerable amount of researches that cannot be all cited here, see however [13–34] and references therein. Among the roles that have been proposed for the Cytb_{559} it has been suggested that it could have a protective role against photoinhibition by taking electron(s) from reduced quinones or Pheo [20–25] thus avoiding the formation of the deleterious singlet oxygen. It has also been proposed that it could be involved in a secondary electron transfer pathway thus avoiding a too large oxidizing power on the electron donor side of PSII [20]. The implication of Cytb_{559} in the repair of PSII after photoinhibition has also been discussed, *e.g.* [34].

Many site-directed mutations in Cytb_{559} have been constructed and studied either in plant PSII, *e.g.* [24], in *Chlamydomonas reinhardtii*, *e.g.* [26–28,34], in the cyanobacterium *Synechocystis* 6803, *e.g.* [29–33] and in *Thermosynechococcus elongatus* [21] (see Fig. S1 in the Supplementary Material for the location of the amino acids already mutated in the literature). One of the challenges was to get mutants with an assembled PSII but lacking the haem with the hope to identify either a structural role for the haem or the electron transfer steps which could be inhibited and therefore would require the haem. Unfortunately, in most of the studied cases, the mutants lacking the haem axial ligands of Cytb_{559} were unable to assemble the PSII making such a study impossible. There was however one exception in which mutants lacking the haem assembled. Indeed, in [26,34] the authors succeeded in making mutants in *C. reinhardtii* on the axial ligand of haem iron of the α subunit: the PsbE/His23Met, PsbE/His23Tyr [26] mutants and the PsbE/His23Cys mutant [34]. Whereas these three mutants could not grow autotrophically, they were able to assemble O_2 evolving PSII up to ≈ 15 % of the wild-type level whereas the purified PsbE/His23Met and PsbE/His23Tyr mutants contained no haem [26] and the PsbE/His23Cys mutant contained a haem at sub-stoichiometric levels [34]. These results lead the authors to conclude that the haem was not absolutely required for the PSII assembly. However, in [26], one question raised by the authors was that the haem content was determined by EPR in purified PSII but not in thylakoids due to the low level of PSII in the membrane. So, since Met and Tyr in [26] and Cys in [34] could be potentially an axial ligand of the haem iron, the possibility that the haem was lost during the PSII purification procedure due to an altered ligation could not be discarded.

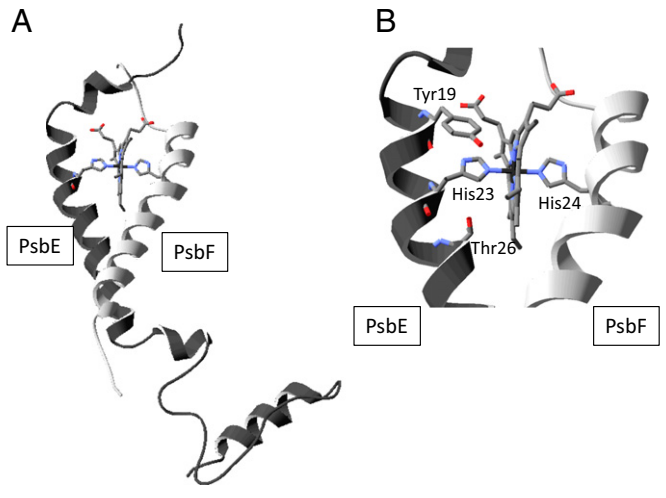

Fig. 1. (A) Structure of Cytb_{559} consists with PsbE, PsbF helicies and a haem from the 1.9 Å model of Umena et al. (1). His23 of PsbE and His24 of PsbF are axial ligand of the haem-Fe. (B) Structure around the haem of Cytb_{559}. Tyr19, His23 and Thr26 of PsbE were amino acid residues that were substituted by Phe, Ala or Met, and Pro for PsbE/Tyr19Phe, PsbE/His23Ala, PsbE/His23Met and PsbE/Thr26Pro, respectively in this study. Structures in Panel A and B were drawn with Swiss Pdb Viewer with the PDB 3ARC structure (1).

It is generally agreed that the oxygen evolution activity in purified PSII from cyanobacteria, in particular from the thermophilic *T. elongatus*, is much more stable than in PSII purified from *C. reinhardtii*. Another advantage of *T. elongatus* is that the structure has been resolved in a very similar cyanobacterium, *T. vulcanus*. However, the great disadvantage of *T. elongatus* is its inability to grow in heterotrophic conditions in contrast to *C. reinhardtii* and *Synechocystis* 6803. Since, so far, this latter species is however unable to assemble PSII in mutants lacking the haem of Cytb_{559} we have nevertheless attempted to make site directed mutants lacking the Cytb_{559} haem in *T. elongatus* with the hope that the robustness of PSII variant with PsbA3 as the D1 subunit would be an asset.

Four mutants have been designed and studied (Fig. 1B). In the PsbE/Tyr19Phe and the PsbE/Thr26Pro mutants, the environment of the PsbE/His23, one of the two haem iron axial ligands, was expected to be modified. Indeed, Tyr19 is involved in the H-bond network around His23 and in the Thr26Pro mutant the PsbE α-helix is expected to be strongly disrupted. In the two other mutants, the PsbE/His23 haem iron axial ligand was substituted for either a Met which potentially could be also a ligand or for an Ala which cannot. We found that the four mutants were able to grow in photoautotrophic conditions. This allowed us to monitor the photoinhibition rate under high-light conditions by measuring the O_2 evolution activity. Moreover, thylakoids and then PSII could be purified with a yield similar to that one in the wild type. This allowed us to study these mutants by MALDI-TOF mass spectrometry and EPR spectroscopies. Indeed, the Cytb_{559} exhibits different redox potential forms: a high-potential (HP) form with a midpoint redox potential (E_m) around +400 mV and forms with lower potentials, ≤ + 280 mV, *i.e.* either intermediate potentials (IP) or low potential (LP), *e.g.* [16,35,36] and references therein). It is of note that each of the IP and LP notations may refer to different potentials depending on the authors. The HP form is labile and easily converted to lower potential forms by treatments that alter the PSII integrity [35,36]. In *T. elongatus* wild type, the E_m of both the HP (≈ + 390 mV) and IP (≈ + 260 mV) forms are not affected by pH, while a pH-dependent behavior has been described for the LP form in plant PSII, [16] and references therein.

At least four EPR forms of Cytb_{559} are detectable; the HP and LP forms both in a non-relaxed and relaxed state, [16,37] and references therein. The non-relaxed HP form of Cytb_{559} with $g_z \approx 3.08$, $g_y \approx 2.16$ and $g_x \approx 1.41$ can be induced by low-temperature (<140 K) illumination of an O_2-evolving sample. The relaxed high-potential form exhibits slightly different g values with $g_z \approx 3.03$, $g_y \approx 2.19$ and $g_x \approx 1.44$ and is induced by an annealing of the sample above 200 K [37]. The non-relaxed LP form of Cytb_{559}, with $g_z \approx 3.05$, $g_y \approx 2.18$ and $g_x \approx 1.46$, is observed in Mn-depleted PSII after illumination at low temperature (<200 K), whereas the relaxed state with $g_z \approx 2.95$, $g_y \approx 2.25$ and $g_x \approx 1.51$ is observed after an annealing of the sample above 200 K. The relaxation process has been interpreted as being possibly a reorientation of the imidazole plan of at least one of the two histidine ligand [37]. Since the IP forms exhibit *g* values intermediate between those of the HP and LP forms there is an apparent correlation between the redox potential of Cytb_{559} and its EPR characteristics, *e.g.* [35,37]; larger is the g_z value higher is the redox potential. This correlation is likely because a high g_z value is synonym of a more distorted structure (*i.e.* a more constrained structure) in the oxidized state, *e.g.* [38] and reference therein. So, the presence of the haem in the four mutants studied here and possibly the redox properties and oxidation level of Cytb_{559} were extrapolated from the EPR characteristics in thylakoids and then in purified PSII.

From these measurements it is confirmed that the haem is not at all required for the PSII assembly since in both the PsbE/His23Met and the PsbE/His23Ala mutants the PSII was fully active whereas the haem (but not the PsbE and PsbF subunits) was lacking. However, in these

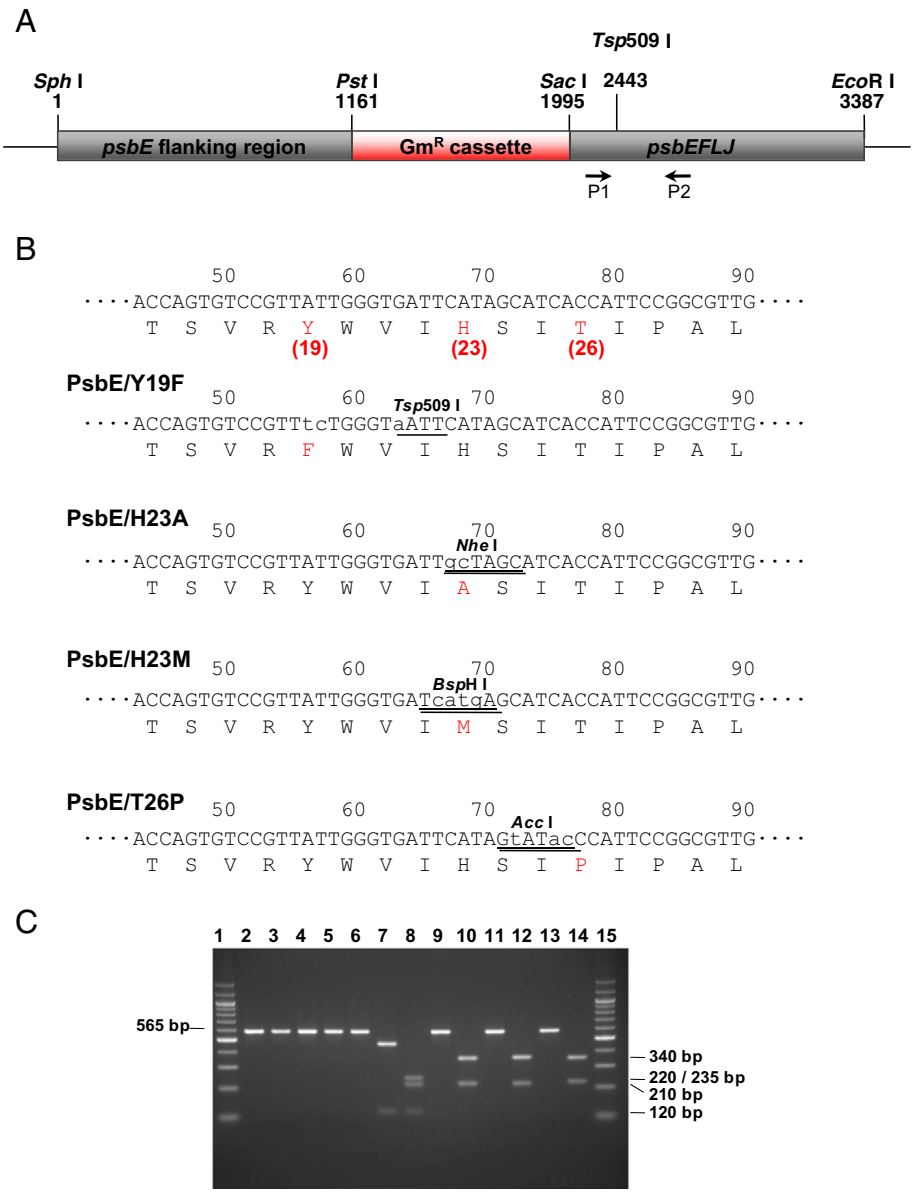

Fig. 2. (A) Map around site-directed *psbE* of *T. elongatus* mutant genome. A gentamycin (Gm) resistant cassette was inserted into 150 bp upstream of the initial codon of *psbEFLJ* cluster at created *Pst* I and *Sac* I sites. (B) The nucleotides and translated amino acids sequences included Tyr19, His23 and Thr26 of wild type and the PsbE mutants. Newly created restriction enzyme sites for site-directed mutations are underlined. *Tsp*509 I, *Nhe* I, *Bsp*H I and *Acc* I sites were newly created in Tyr19Phe, His23Ala, His23Met and Thr26Pro mutants of PsbE, respectively. Small characters are substituted nucleotides for mutations. (C) Agarose gel (1%) electrophoresis of amplified products by PCR using *P1* and *P2* primers indicated in Fig. 2A (lanes 2 - 6), and digested the amplified DNA fragments with *Tsp*509 I (lanes 7 and 8), *Nhe* I (lanes 9 and 10), *Bsp*H I (lanes 11 and 12) and *Acc* I (lanes 13 and 14). Lanes 2, 7, 9, 11 and 13, WT*3; lanes 3 and 8, Y19F mutant; lanes 4 and 10, His23Ala mutant; lanes 5 and 12, His23Met mutant; lanes 6 and 14, Thr26Pro mutant; lanes 1 and 15, 1 kb DNA ladder markers (Nakarai Co., Japan).

mutants, the PSII in whole cells was shown to be repaired/assembled more slowly under photoinhibitory conditions.

1. Materials and methods

1.1. T. elongatus mutant strains

The PsbE mutants were constructed in *T. elongatus* WT*3 cells, *i.e.* in a strain in which the $psbA_1$ and $psbA_2$ genes have been deleted [39]. In addition, a His_6-tag on the C-terminus of CP43 mutants has been added [40]. DNA fragments including about 1300 bp of 5′-flanking region of *psbE* and about 1250 bp including a *psbEFLJ* cluster were subcloned into pUC19 plasmid at *Sph* I and *Eco*R I sites. Then, a gentamycin (Gm) resistant cassette (≈1800 bp) [41] was inserted 140 bp upstream of the initial codon of *psbE* at *Pst I* and *Sac* I sites. Fig. 2A shows the construction map of this plasmid for transformation of *T. elongatus*. For creation of site-directed mutations on PsbE, newly restriction enzyme sites were created by using a Quick-Change Lightning Site-Directed Mutagenesis Kit (Stratagene). As shown in Fig. 2B, *Tsp*509 I, *Nhe* I, *Bsp*H I and *Acc* I recognitions were created for PsbE/Tyr19Phe, PsbE/His23Ala, PsbE/His23Met and PsbE/Thr26Pro mutants, respectively. The *T. elongatus* transformants were selected as single colonies on DTN agar plate containing appropriate antibiotics (spectinomycin 25 μg mL^{-1}, streptomycin 10 μg mL^{-1}, kanamycin 40 μg mL^{-1} and gentamycin 25 μg mL^{-1}). Segregation of all genome copies was confirmed by digestion of amplified 565 bp of DNA fragments including the site-directed mutations by *P1* primer (5′-GAGCTCCCTCAAAGAGGGCATCATCT-3′) and *P2* primer (5′- GGTTCCATGGGTGCACCCTCCTAACGTTGG-3′) with *Tsp*509 I, *Nhe* I,

*Bsp*H I and *Acc* I for Tyr19Phe, His23Ala, His23Met and Thr26Pro mutants of PsbE, respectively (data shown in Fig. 2C).

1.2. Isolation of thylakoids and PSII complexes

Mutant cells were grown in 1 L of DTN in 3–L Erlenmeyer flasks in a rotary shaker with a CO_2–enriched atmosphere at 45 °C under continuous light (≈80 μmol of photons m^{-2} s^{-1}) until they reached an optical density (O.D.) close to 1.0 at 800 nm. After harvesting by centrifugation, the cells were washed and resuspended in 10 % glycerol, 1 M betaine, 40 mM MES, 15 mM $MgCl_2$, 15 mM $CaCl_2$, pH 6.5 adjusted with NaOH. After the breakage of the cells with a French Press, thylakoids were prepared as described earlier [42,43]. The PSII core complexes were then isolated from solubilized thylakoids by Ni^{2+}-affinity chromatography as described earlier [38,39]. PSII core complexes were finally resuspended in 1 M betaine, 40 mM MES, 15 mM $MgCl_2$, 15 mM $CaCl_2$, pH 6.5, at a Chl concentration of ≈ 1.5–2.0 mg Chl mL^{-1} and stored in liquid N_2 before to be used.

For the tris-washing, the PSII were diluted approximately 10-fold in a medium containing 1.2 M Tris-HCl (pH 9.2) and were incubated under room light at 4 °C for 1 h. The samples were then collected by centrifugation at 600,000 *g* for 3 h. Then, the pellets were resuspended in 1 M betaine, 40 mM MES, 15 mM $MgCl_2$, 15 mM $CaCl_2$, pH 6.5. After a second centrifugation, 600,000 *g* for 3 h, the pellet was resuspended in the same medium at ≈ 1.5–2.0 mg Chl mL^{-1} and stored in liquid N_2 before to be used.

1.3. Incubation of cells under high-light conditions

To get cells in as much as possible similar physiological states they were pre-cultivated until $O.D._{730}$ ≈ 0.6, *i.e.* in the exponential phase. Cultivation was done at 45 °C under continuous white light (≈60 μmol of photons m^{-2} s^{-1}, aquarium type for the fluorescent tubes) in a rotary shaker (120 rpm). Just before the analyses, the cells were diluted to $O.D._{730}$ = 0.3 (30 mL final volume) into 50-mL Erlenmeyer flasks. High light illumination was done with fluorescent light tubes (Toshiba Plantlux, Japan, with an emission spectrum more intense between 600 and 700 nm and between 400 nm and 500 nm) with a light intensity equal to ≈ 800 μmol of photons m^{-2} s^{-1} for 4 h. Then, the light intensity was decreased to ≈ 60 μmol of photons m^{-2} s^{-1} for 2 h. When added, the concentration of lincomycin in the culture was adjusted to 200 μg mL^{-1}. It has been checked that 400 μg mL^{-1} of lincomycin resulted in similar results showing that the 200 μg mL^{-1} used here was saturating.

1.4. Oxygen evolution measurements of whole cells incubated under high light conditions

Thirty mL of *T. elongatus* cells were quickly took out from the culture and then harvested by centrifugation. After the washing of the cells in 40 mM MES buffer (pH 6.5) containing 15 mM $CaCl_2$, and 15 mM $MgCl_2$, and 20 mM NaCl, they were suspended in the same buffer at a concentration of ≈ 5 μg of Chl mL^{-1}. Oxygen evolution was measured at 25 °C by polarography using a Clark type oxygen electrode (Hansatech) with saturating white light through infrared and water filters. The activity was measured over a period of 1.5 minute in the presence of 1 mM 2,6-dichloro-*p*-benzoquinone (DCBQ) dissolved in dimethyl sulfoxide as an electron acceptor.

1.5. SDS-polyacrylamide gel electrophoresis

PSII complexes suspended in 40 mM MES/NaOH (pH 6.5), 10 mM NaCl, 10 mM $CaCl_2$, 10 mM $MgCl_2$, 0.03% *n*-dodecyl-β-D-maltoside were solubilized with 2% lithium laurylsulfate, and then analyzed by SDS-polyacrylamide gel electrophoresis with a 16–22% gradient gel containing 7.5 M urea as described in [44].

1.6. MALDI-TOF/mass spectrometry

MALDI-TOF/MS measurements were done as described earlier [45]. The isolated PSII complexes (150 μg of Chl mL^{-1}) were mixed with the same volume of a saturated matrix (sinapic acid, Fluka) solution that consisted in 60% acetonitrile and 0.1% trifluoroacetic acid. MALDI-TOF/MS analysis was performed using a Voyager-DE PRO MALDI-TOF/MS spectrometer (Applied Biosystems). The instrument was operated in reflector mode at a 20-kV accelerating voltage and 100-ns ion extraction delay with the nitrogen laser working at 337 nm and 3 Hz. One hundred laser flashes were accumulated per spectrum. The *m/z* values in Fig. 3 resulted from the average of hundred spectra. Internal calibration was performed on the samples premixed with human adrenocorticotropic hormone fragment (from Sigma, $m/z = 2466.72$), with bovine insulin (from Sigma, $m/z = 5734.51$) and bovine heart apomyoglobin (from Sigma, $m/z = 16952.27$).

1.7. EPR spectroscopy

CW-EPR spectra were recorded using a standard ER 4102 (Bruker) X-band resonator with a Bruker Elexsys 500 X-band spectrometer equipped with an Oxford Instruments cryostat (ESR 900). The thylakoids at 3–4 mg Chl mL^{-1} and PSII samples at ≈ 1-2 mg Chl mL^{-1} were loaded in the dark into quartz EPR tubes and further dark-adapted for 1 h at room temperature. Then, the samples were frozen in the dark to 198 K and then transferred to 77 K in liquid N_2. Prior to the measurements all the samples were degassed at 198 K. Illuminations with visible light for approximately 5–10 seconds with a 800 W tungsten lamp filtered by water and infrared cutoff filters were done in a non-silvered dewar filled either with ethanol cooled down with dry ice for illumination at 198 K or with liquid N_2 for illumination at 77 K.

2. Results

Fig. 3 shows the polypeptide content in PSII from WT*3 cells and from the four PsbE mutant cells analyzed by SDS-polyacrylamide gel electrophoresis (Panel A) and MALDI-TOF/MS (Panels B and C). These data show that in the four mutants there were neither additional subunits nor missing subunits except PsbY. Indeed, from the MALDI TOF spectra, PsbY was partially or completely removed from PsbE/His23Ala-PSII, PsbE/His23Met-PSII and PsbE/Thr26Pro-PSII. It is known that PsbY is weakly bound to PSII complex. The PsbY subunit locates close to PsbE in the PSII complex [2,3] (Fig. S6) and it was also missing in the PSII crystal at 1.9 Å resolution [1] and in the PsbJ knockout mutant [45] but was present in crystals of Sr containing PSII [2]. Therefore, the partial or total lack of PsbY observed here in PsbE/His23Ala-PSII, PsbE/His23Met-PSII and PsbE/Thr26Pro-PSII suggests a weaker binding of this subunit when compare to WT*3-PSII likely due to slight structural modifications of Cytb_{559}. Importantly, Fig. 3 shows that both PsbE (Cytb_{559} α subunit) and PsbF (Cytb_{559} β subunit) were stoichiometrically bound to PSII in the four site-directed mutants by comparison with the PsbE and PsbF contents in WT*3-PSII. Panel C shows the PsbE peak on an extended *m/z* scale. The *m/z* values for the wild type PsbE (calculated, 9441.5 Da; experiment, 9442 Da), for PsbE/Tyr19Phe (calculated, 9425.5 Da; experiment, 9425 Da), for PsbE/His23Ala (calculated, 9375.5 Da; experiment, 9375 Da), for PsbE/His23Met (calculated, 9435.6 Da; experiment, 9435 Da) and PsbE/Thr26Pro (calculated, 9437.5 Da; experiment, 9435 Da) thus showing that the PsbE subunits inserted into PSII were indeed the mutated ones.

Panels A and B in Fig. 4 show the g_z magnetic field region of light-induced EPR spectra recorded in untreated thylakoids and untreated PSII, respectively. Spectra were first recorded in dark-adapted samples and then after illumination at 77 K (the spectra recorded before and after the illumination in thylakoids are shown in Fig. S2 and in Fig. S4 for purified PSII. Fig. S3 shows the spectra in thylakoids after

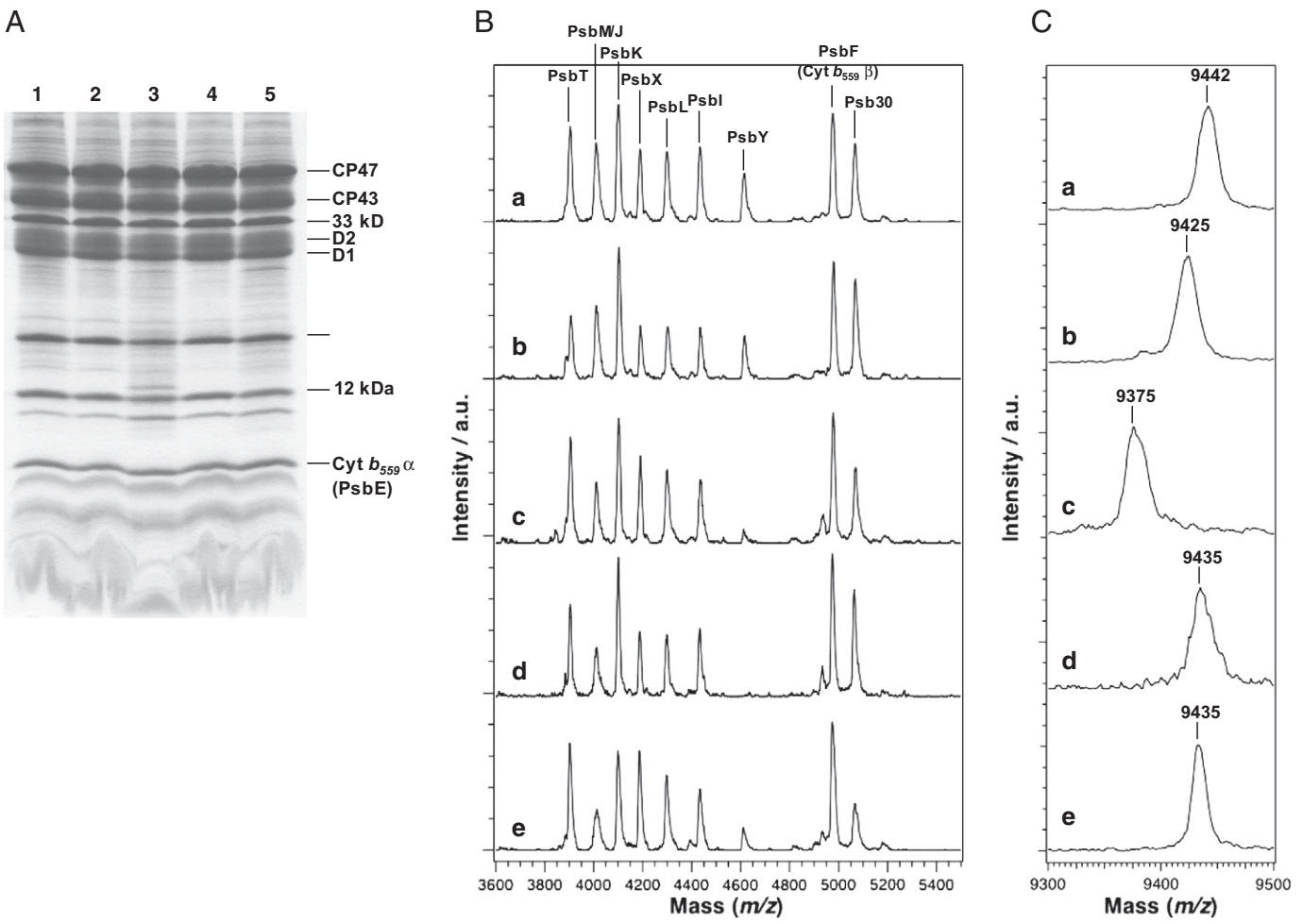

Fig. 3. Analyses of isolated PSII complexes from WT*3 and PsbE mutants with SDS-polyacrylamide gel electrophoresis (Panel A) and MALDI-TOF/mass spectrometry (Panels B and C). (A) Lane 1, WT*3; lane 2, PsbE/Tyr19Phe; lane 3, PsbE/His23Ala; lane 4, PsbE/His23Met; lane 5, PsbE/Thr26Pro. Each lane was loaded with 8 μg Chl of PSII sample. The gel was stained with Coomassie Brilliant Blue R-250. (B) MALDI-TOF mass spectra of isolated PSII complexes from WT*3 (spectrum a), PsbE/Tyr19Phe (spectrum b), PsbE/His23Ala (spectrum c), PsbE/His23Met (spectrum d) and PsbE/Thr26Pro (spectrum e) in the *m/z* range from 3600 to 5400. (C) MALDI-TOF mass spectra focused on PsbE polypeptides in the *m/z* range from 9300 to 9500. Spectrum a, WT*3; spectrum b, PsbE/Tyr19Phe; spectrum c, PsbE/His23Ala; spectrum d, PsbE/His23Met; spectrum e. PsbE/Thr26Pro.

illumination and subtraction of the baseline). The light-*minus*-dark spectra shown are expected to be free from the spectral contribution of Cytc_{550} the spectrum of which remaining unaltered upon illumination when spectra are recorded with non-saturating microwave powers. In thylakoids, signals from the light-induced reduced PSI iron sulfur clusters did not allow us to detect the g_y and g_x features of Cytb_{559}. In the thylakoids and PSII of WT*3 (black spectra), the light-*minus*-dark spectra exhibited a g_z value of 3.07 that is characteristic of the HP non-relaxed form of Cytb_{559}. A light-induced spectrum with a similar g_z value was observed in the PsbE/Tyr19Phe mutant (orange spectra) showing that this mutation hardly affects the EPR properties and therefore very likely the redox properties of Cytb_{559}. At odds with this observation, the larger amplitude of the light-induced signal in the thylakoids from WT*3 than in thylakoids from PsbE/Tyr19Phe could nevertheless indicate that the proportion of reduced Cytb_{559} was smaller in the mutant which, in turn, could suggest a change in the Em. However, the accurate determination of a g_z value is simpler than that of the amplitude of a light-induced cytb_{559} signal and this discrepancy could be due to the difficulty of such measurements in thylakoids. The green spectrum in Panel A shows the light-induced signal in the PsbE/Thr26Pro thylakoids. In this mutant, the g_z value was downshifted to 2.98. This downshift suggests a decrease in the E_m value of the Cytb_{559} in this mutant. The absence of any detectable light-induced signal in PsbE/Thr26Pro PSII (not shown) indicates that the E_m value of the Cytb_{559} in this mutant was likely further decreased during the PSII purification procedure so that the Cytb_{559} was already fully oxidized in the dark-adapted sample. After the addition of 5 mM ascorbate, a very small light-induced signal seemed to be detectable with a g_z value close to 2.98 (green spectrum in Fig. 4B). This could indicate that in the PsbE/Thr26Pro PSII sample the oxidized Cytb_{559} was reducible by ascorbate only in a very low minority of centers suggesting an E_m value much lower than that of ascorbate. Finally, in the PsbE/His23Ala mutant (red spectra) and PsbE/His23Met mutant (blue spectra) no signal was induced by the 77 K illumination both in thylakoids and in purified PSII, even after the addition of 5 mM ascorbate (not shown). So, the Cytb_{559} was either already fully oxidized prior to the 77 K illumination or not oxidable or, more likely, the haem was laking in these mutants. Indeed, as shown in Fig. S3, in the magnetic field region where the g_z signal from both Cytc_{550} and Cytb_{559} contribute, the signal amplitude in PsbE/His23Met-PSII and PsbE/His23Ala-PSII was half of that in the other sample suggesting that the signal from Cytb_{559} was missing. However, because the superimposition of the spectrum of the oxidized Cytc_{550} in the dark adapted samples makes difficult the answer to this question, a tris-washing of the PsbE/His23Met-PSII and PsbE/His23Ala-PSII has been performed to remove the Cytc_{550} [40] and to spectroscopically clarified this magnetic field region.

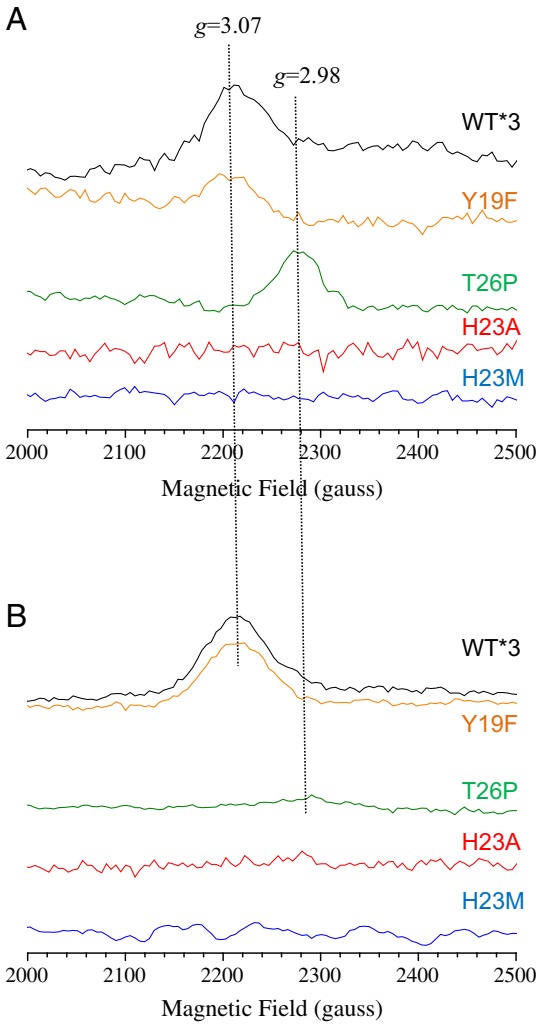

Fig. 4. EPR spectra in the g_z spectral range of cytochromes in purified membrane fragments (thylakoids) (panel A) and in purified PSII (panel B). EPR spectra were recorded in WT*3 (black spectra) in the PsbE/Tyr19Phe mutant (orange spectra), in the PsbE/Thr26Pro mutant in the presence of 5 mM ascorbate (green spectra), in the PsbE/His23Ala mutant (red spectra) and in the PsbE/His23Met mutant (blue spectra). The spectra are the light-*minus*-dark spectra induced by illumination at 77 K. Instrument settings: modulation amplitude, 25 gauss; microwave power, 5 mW; microwave frequency, 9.4 GHz; modulation frequency, 100 kHz. Temperature, 15 K. Amplitude of the spectra was normalized to same reaction center concentration by using the $Tyr^{\bullet}_{D}$ EPR signal as a probe. The different signal-to-noise ratio of the spectra is due to the use of samples with different Chl concentration.

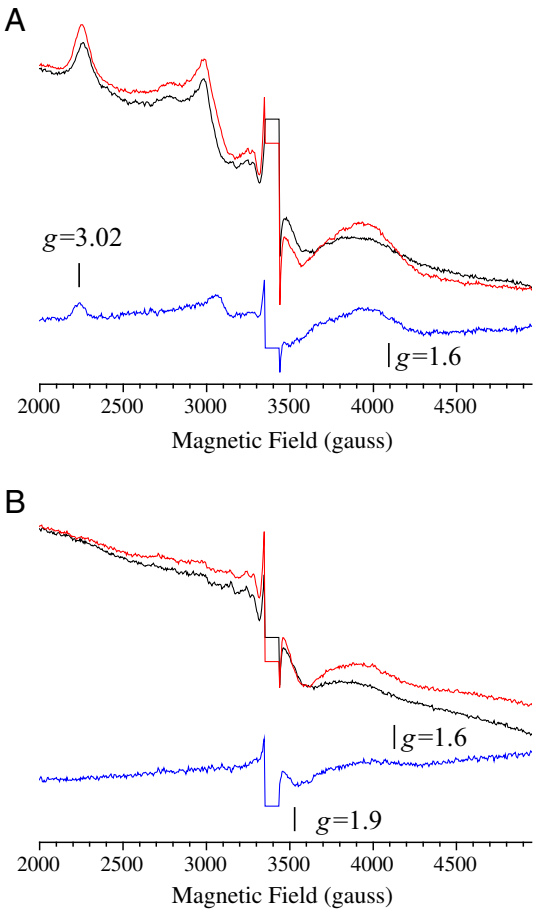

Fig. 5. EPR spectra in the spectral range of cytochromes in purified WT*3-PSII (Panel A) and PsbE/His23Ala-PSII (panel B). The spectra were recorded in dark-adapted samples without any addition (black spectra) and after illumination at 77 K (red spectra). The blue spectra are the light-minus-dark spectra induced by illumination at 77 K. Instrument settings: modulation amplitude, 25 gauss; microwave power, 5 mW; microwave frequency, 9.4 GHz; modulation frequency, 100 kHz. Temperature, 15 K. Amplitude of the spectra was normalized to same reaction center concentration by using the $Tyr^{\bullet}_{D}$ EPR signal as a probe. The spectral region corresponding to the $Tyr^{\bullet}_{D}$ EPR signal has been deleted.

Fig. 5 shows the spectra recorded before (black spectra) and after (red spectra) an illumination at 77 K in tris-washed WT*3-PSII (Panel A) and in tris-washed PsbE/His23Ala PSII (Panel B). The blue spectra are the light-*minus*-dark spectra. In tris-washed WT*3 PSII, the spectrum recorded in the dark-adapted state shows that a large fraction of the Cytb_{559}, likely in a relaxed IP form taking into account a g_z value close to 3.0, was already oxidized. The detection of a light-induced signal indicates that in a low proportion of centers the Cytb_{559} was nevertheless reduced in the dark-adapted state and then oxidized by the illumination. The g_z value of 3.02 for the light-induced spectrum is indicative of a non-relaxed oxidized IP form. In this sample, the g_x signal was not detected due to the superimposition of the large light induced $Q_A^- Fe^{II} Q_B^-$ signal detected at magnetic fields above 3500 gauss (signal at $g = 1.6$). In the tris-washed PsbE/His23Ala PSII any Cytb_{559} signal was detected neither before nor after the 77 K illumination. Only the light-induced quinone signals at $g = 1.9$ ($Q_A^- Fe^{II} Q_{B)}$ and $g = 1.6$ ($Q_A^- Fe^{II} Q_B^-$) were detected in the magnetic field range shown).

Since the PsbE/His23Met and PsbE/His23Ala mutants were able to grow under photo-autotrophic conditions, they are necessarily able to evolve oxygen. The oxygen-evolving activities under continuous saturating light are given for whole cells and purified PSII in Table 1. Both in whole cells and purified PSII the oxygen-evolving activity was found similar in WT*3 and in the PsbE/Thr26Pro mutant thus showing a lack of correlation between the changes in the EPR properties of Cytb_{559} in the mutant (see above) and the O_2 activity. In the 3 other mutants the activity was decreased to reach ≈ 50 % of that in the WT*3 in purified PsbE/His23Met and PsbE/His23Ala. The PSII content relatively to the Chl concentration was nevertheless found to be similar in PsbE/His23Ala for example as estimated from the amplitude of the $Tyr^{\bullet}_{D}$ EPR

Table 1
Oxygen-evolving activity in whole cells and purified PSII of WT*3 and PsbE mutants. These values results from triplicate measurements with 3 different batches of cells, and triplicate measurements with isolated PSII.

Strain	Cells μmol O_2 (mg Chl)$^{-1}$ h^{-1} (% relatively to WT*3)	Purified PSII μmol O_2 (mg Chl)$^{-1}$ h^{-1} (% relatively to WT*3)
WT*3	338 ± 12 (100%)	3470 (100%)
PsbE/Y19F	252 ± 38 (75 %)	2800 (81%)
PsbE/H23A	245 ± 16 (72 %)	1850 (53%)
PsbE/H23M	256 ± 23 (76 %)	1790 (52%)
PsbE/T26P	335 ± 15 (99 %)	3550 (102%)

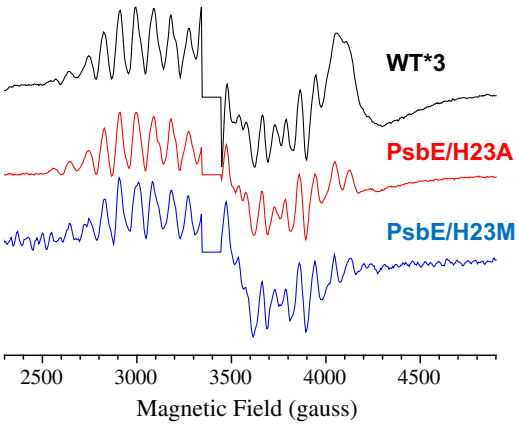

Fig. 6. Light-*minus*-dark EPR spectra induced by 200 K illumination of dark adapted samples. phenyl-*p*-benzoquinone (0.5 mM) was added before the freezing of the samples. Black spectrum, WT*3-PSII; red spectrum, PsbE/His23Ala-PSII; blue spectrum, PsbE/His23Met-PSII. Instrument settings: modulation amplitude, 25 gauss; microwave power, 20 mW; microwave frequency, 9.4 GHz; modulation frequency, 100 kHz. Temperature, 8.6 K. Amplitude of the spectra was normalized to same reaction center concentration by using the $Tyr^{\bullet}_{D}$ EPR signal as a probe. The spectral region corresponding to the $Tyr^{\bullet}_{D}$ EPR signal has been deleted.

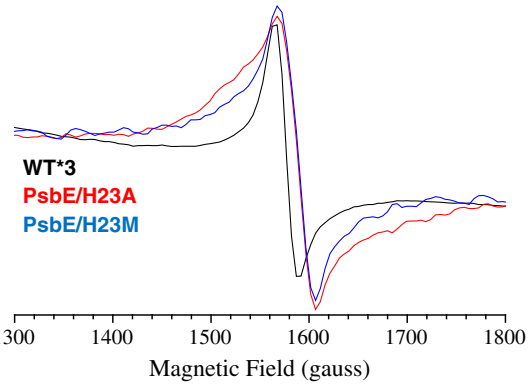

Fig. 7. EPR spectra in the magnetic field region corresponding to the rhombic Fe^{3+} signal and without any addition. Black spectrum, WT*3-PSII; red spectrum, PsbE/His23Ala-PSII; blue spectrum, PsbE/His23Met-PSII. Same instrument settings as in Fig. 6. Amplitude of the spectra was normalized to same reaction center concentration by using the $Tyr^{\bullet}_{D}$ EPR signal as a probe.

signal (see Fig. S5). The lower activity in purified mutant PSII is more probably due to a less stable complex during purification rather to an intrinsic defect (see below for an alternative explanation).

Formation of the S_2 EPR multiline signal was then monitored in the two mutants in which the haem was lacking. Fig. 6 shows the signals light-induced at 200 K in WT*3-PSII, in the PSII of the PsbE/His23Ala mutant and in the PSII of the PsbE/His23Met mutant. The only difference in the 3 samples is the $Q_A^- Fe^{II} Q_B^-$ signal [46] that was detected in the WT*3 sample whereas a larger $Q_A^- Fe^{II} Q_B$ or $Q_A^- Fe^{II}$ signal seemed present at least in the PsbE/His23Met mutant. From our experience on PSII from *T. elongatus*, the redox state of the quinones may differ from sample to sample and the results in Fig. 6 alone do not allow us to conclude on a possible role of the haem of Cytb_{559} on the redox state of the quinones Q_A and Q_B. Further experiments are required to test such a possibility. The main result in Fig. 6 is that the amplitude of the S_2 multiline signal induced by 200 K illumination in both the PsbE/His23Ala and PsbE/His23Met mutants was similar to the amplitude of the S_2 multiline signal in WT*3-PSII with also no change in the spectral properties indicating no modification in the environment of the Mn_4CaO_5 cluster. These results indicate that the lower O_2 evolution activity in the purified mutant PSII mentioned above was due in part to a slowdown of one electron transfer step on the acceptor side rather than to a decrease in the proportion of centers having an intact Mn_4CaO_5 cluster.

Several arguments, taken together, show that the lack of the Cytb_{559} haem did not prevent the assembly of active PSII in whole mutant cells. Otherwise, we would have either inactive purified PSII or (if inactive PSII cannot be purified because they would be disintegrated during the purification procedure) a smaller amount of purified PSII in mutants. Indeed; *i*) from the $Tyr^{\bullet}_{D}$ signal in whole cells (Fig. S5) the amount of PSII (active and inactive if they exist) is similar in WT*3 cells and mutant cells on a Chl amount basis, *ii*) the O_2 activity is similar in WT*3 and mutant cells also on a Chl amount basis showing that they is no inactive PSII (Table 1), *iii*) the yield of the PSII purification procedure was similar in WT*3 and in the PsbE/His23Ala and the PsbE/His23Met mutants mutant cells (not shown).

In [26] the authors suggested that in *C. reinhardtii*, with a disrupted haem binding pocket, a chlorophyll molecule could substitute for the haem thus helping in the structural stabilization of the PsbE and PsbF subunit. Fig. 7 shows the EPR spectra recorded in WT*3-PSII, PsbE/His23Ala-PSII and PsbE/His23Met-PSII in a magnetic field region where the rhombic Fe^{3+} contributes. The two mutants exhibit a slightly larger and different signal than that one recorded in WT*3 PSII suggesting that, in a minority of centers lacking the haem, the binding of a Fe^{3+} in place of the haem could occur. In this case, the PsbF/His24 could be a ligand of this non-haem iron (schematized in Fig. S6B).

From the data above, it seems unambiguous that PSII with the PsbE and PsbF subunits present but lacking the haem can be assembled in an oxygen-evolving PSII core complexes. So, a structural role as a major role for the haem can be reasonably discarded at least if we consider only the steady-state level of active PSII and not the kinetics at which PSII is assembled (see below). The second possibility mentioned in the literature for the role of Cytb_{559} was either a protection against the photoinhibition process or a faster recovery upon this photoinhibition. To get new insights on this question, oxygen evolution activity in WT*3 cells and in the PsbE mutant cells were measured during high-light conditions (Fig. 8A). The oxygen evolution activity of both PsbE/Tyr19Phe (orange) and PsbE/Thr26Pro (green) cells was inhibited by high light irradiation (800 μmol of photons m^{-2} s^{-1}) in 1 h to reach an activity close to 70% of the initial activity. Then, increasing the duration of the high light illumination did not further decrease the O_2 evolution activity. This inhibition pattern was very similar to that of WT*3-cells (black). However, when the light intensity was reduced to an intensity corresponding to growth light (60 μmol of photons m^{-2} s^{-1}), the activity of both the PsbE/Tyr19Phe and PsbE/Thr26Pro mutant cells did not recover to an extent similar to that one observed for WT*3 cells. For the PsbE/His23Ala (red) and PsbE/His23Met (blue) mutant cells, the oxygen evolution activity decreased in 1 h to reach a level close to ≈ 50% of the initial one. After 3 hours of high-light illumination, a level corresponding to ≈ 40% of the initial activities was reached and remained stable. After the high-light damages, the activity of the PsbE/His23Ala and PsbE/His23Met mutant cells did not recover under growth light conditions.

The activities measured in Fig. 8A are the resultant of the photoinhibition rates with the assembly rates of newly generated active PSII. To estimate the degradation rates alone, a similar experiment to that in Panel A has been performed in the presence of lincomycin, an inhibitor of protein synthesis. As shown in Fig. 8B, the inhibition rate of the initial oxygen-evolving activity of the four PsbE mutant cells was very similar to that of WT*3 cells with a kinetics much faster than in the absence of lincomycin for all the strains. These results strongly suggest that the assembly of active PSII complexes lacking the haem (PsbE/His23Ala and PsbE/His23Met) is slower than in the PsbE/Tyr19Phe and PsbE/Thr26Pro mutants and of course than in the WT*3 but that this assembly nevertheless occurs as evidenced by the steady state level of the activity in Panel A after 2 hours under high light irradiation conditions. In agreement with what it precedes, the growth rates of the four mutants when compared to the WT*3 strain were found similar under low light conditions whereas for PsbA/His23Ala and PsbE/His23Met

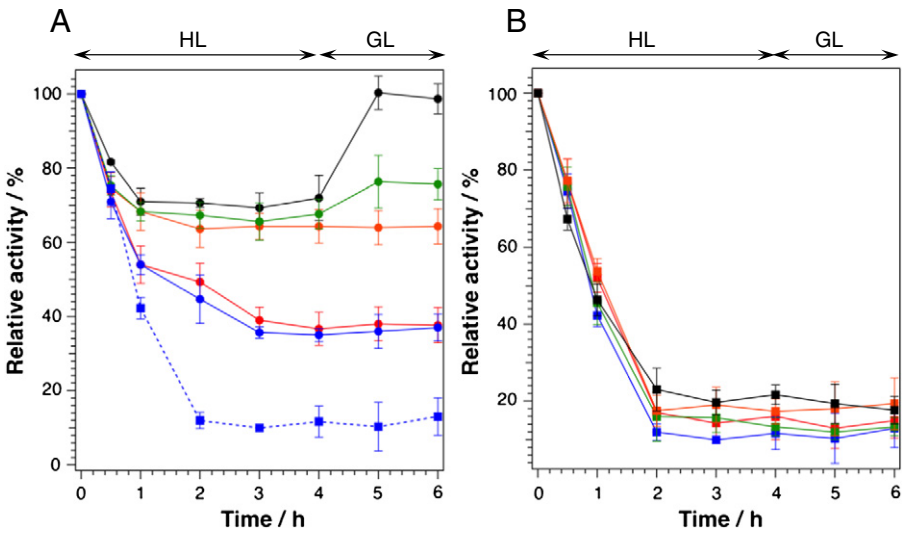

Fig. 8. Relative oxygen-evolving activity of WT*3 and Cytb_{559} mutant cells in the absence (A) and presence (B) of lincomycin. After incubation of the cells under the high light conditions (HL; 800 μmol of photons m^{-2} s^{-1}) for 4 h at 50 °C, the light intensity was decreased to growth light conditions (GL; 60 μmol of photons m^{-2} s^{-1}). The activities are indicated in percentage relatively to the activities at 0 h. The value of the activities were range from 260 to 320 μmol O_2 (mg Chl)$^{-1}$ h^{-1} in cells of WT*3 and all PsbE mutants. Black, WT*3; orange, PsbE/Tyr19Phe; red, PsbE/His23Ala; blue, PsbE/His23Met and green, PsbE/Thr26Pro. Dotted line in (A) is the results of His23Met in the presence of lincomycin. The results of five independent experiments with different batches of cells have been averaged and the activity of each batch of cells have been measured 5 times. The error bars indicate the corresponding standard errors (n = 5).

mutants doubling time was twice that in the other 3 strains (see Table S1 in the supplementary material).

3. Discussion

To get pieces of information on the role of Cytb_{559} in PSII assembly and function, several site-directed mutants have already been described in the literature. Two kinds of mutants have been constructed: i) mutants lacking one of the two histidine born by PsbE and PsbF and which each acts as one of the two haem iron axial ligands and ii) site directed mutations aiming at probing the role of some amino acids in the vicinity of the haem (Figs. 1B and S1).

In the present study, we have also studied these two classes of mutants in *T. elongatus*, something that was not done until now, with the hope that the robustness of the PSII from this organism allows us to get new insights on the role of Cytb_{559}. Four mutants have been designed and studied (Fig. 1B). In two of them, the PsbE/His23 that is one of the two axial ligands of the haem iron was substituted for either a Met which potentially could also be a ligand or for Ala which cannot. In the other two, the PsbE/Tyr19Phe and PsbE/Thr26Pro, the environment of the PsbE/His23 axial ligand of the haem iron was expected to be modified.

In *Synechocystis* 6803, it was observed that mutation of the PsbE/His22 (Pakrasi et al. used His22 in [30], but this His is the 23rd amino acid from the initial Met) reduced the D1 content to a trace level with a PsbE subunit 1.5 kDa smaller. Also in *Synechocystis* 6803, the PsbE/His22Lys mutation resulted in PSII in which the haem of Cytb_{559} was present predominantly in a LP or IP form and in a high spin state in a very low percentage of centers (from the very small amplitude of the $g \approx 6$ EPR signal), *i.e.* likely in a penta-coordinate state in these centers. This PSII was also reported to be easily photoinhibited [32]. The steady state level of PSII in the PsbE/His22Lys mutant was reported to be 81 % of that in the wild type [31]. The other mutations, PsbE/His22Tyr, Cys,Arg,Asp,Met,Gln resulted in a very low amount of PSII which was in addition inactive [31]. In *C. reinhardtii*, as indicated in the Introduction section, the PsbE/His23Met [26], PsbE/His23Tyr [26] and PsbE/His23Cys [34] mutants could not grow photoautotrophically. These mutants were nevertheless able to assemble O_2 evolving PSII up to 15 % of the wild-type level whereas the purified PSII mutants contained either no haem in [26] or contained a haem at a stoichiometric level in [34]. These results lead the authors to conclude that the haem was not absolutely required for the PSII assembly. However, the possibility that the haem was lost during the PSII purification could not be discarded since Met, Tyr and Cys could be potentially an axial ligand of haem iron.

Among the site directed mutants in the vicinity of the haem already studied we can cite the PsbE/Arg17Asp,Leu,Ala in *Synechocystis* 6803 [29], and the equivalent PsbE/Arg18Asp or Arg18Glu in *C. reinhardtii* [27], the PsbE/Tyr18Ser in *Synechocystis* 6803 [32], the PsbE/Arg7Leu in *Synechocystis* 6803 [33] and the PsbE/Ser24Phe in *C. reinhardtii* [28]. In *T. elongatus* [21], the midpoint redox potential of the high potential form was significantly altered in the PsbE-Arg18Ser and PsbE-Ile27Thr mutant strains. The PsbE-Arg18Ser strain also showed a high sensitivity to high light illumination and an altered oxidase activity. Consequently, it was proposed that the extremely positive redox potential of the HP form of Cytb_{559} could be necessary to ensure efficient oxidation of the plastoquinone pool. In addition to specific spectroscopic changes of Cytb_{559} that will not be reviewed here, one common feature observed for all these mutants was a larger photoinhibition of PSII under high-light conditions.

From the present study in *T. elongatus* several observations can be done. Firstly, both the PsbE/His23Met and PsbE/His23Ala mutants are able to grow in phototrophic conditions despite the lack of the haem of Cytb_{559}. The apo-Cytb_{559} was detected in similar amount to that in the wild type with possibly a non-haem Fe^{3+} bound to PsbF/His24 in a small fraction of PSII centers. Clearly, the haem is not required for a proper assembly of an active PSII in a sufficient amount to sustain a phototrophic growing. This differs from what was observed in *Synechocystis* 6803 [30] but is in agreement with what was observed in *C. reinhardtii* [26] although in this species the PSII content was likely too low to allow the cells to grow in phototrophic conditions. So, for the first time, active PSII lacking the haem of Cytb_{559} is available in sufficient amount to allow spectroscopic studies.

Secondly, the EPR properties and therefore possibly the redox properties of the holo-Cytb_{559} are not affected by the PsbE/Tyr19Phe mutation. This contrasts in part with the effect of the corresponding mutation in *Synechocystis* 6803 [32] where the Cytb_{559} was converted

into a low potential form with also a small fraction of PSII centers exhibiting a high spin form. So, the destabilisation of Cytb_{559} after similar mutations involving either the PsbE axial ligand or the environment of the PsbE axial ligand in *Synechocystis* 6803 are not observed in *T. elongatus*. However, since the recovery after photoinhibition is affected in the PsbE/Tyr19Phe mutant in *T. elongatus*, a minor structural role of PsbE/Tyr19 in the PSII assembly cannot be discarded. The differences between *Synechocystis* 6803 and *T. elongatus* could originate from either the presence of PsbA3 which stabilizes the PSII reaction center [45] and/or the slightly different primary sequence of PsbE and PsbF in the two species which would result in a slightly different H-bond network and which in turn would affect the affinity of PsbE/His23 for the haem iron.

Thirdly, the PsbE/Thr26Pro mutation is responsible for the conversion of the high potential form of Cytb_{559} into a low potential form. Further QM/MM theoretical works could determine if this conversion is either due to a change in the electrostatic environment or due to a bending of the α-helix as a consequence of the insertion of a proline residue.

Finally, the four mutant cells were submitted to high-light conditions and the photoinhibition and recovery rates were estimated and compared to those of the WT*3 cells by measuring the O_2 evolution activity. In the presence of the protein synthesis inhibitor lincomycin, the oxygen evolution activity of the four PsbE mutant cells decreased similarly to that one of WT*3 cells under high-light conditions. Therefore, the rate of photoinhibition does clearly not depend neither on the redox potential of the Cytb_{559} nor on the presence or the absence of the haem. This result slightly differs from the *C. reinhardtii* case in which the PsbE/His23Cys [34] and PsbE/His23Tyr [26] mutations resulted in a faster photoinhibition. In *T. elongatus*, in the absence of lincomycin, the strains behaved differently and the steady state percentage of centers affected by high light illumination followed the order PsbE/His23Met ≈ PsbE/His23Ala > > PsbE/Tyr19Phe ≥ PsbE/Thr26Pro ≥ WT*3. When the light intensity was reduced to an intensity corresponding to growth light, the activity of both PsbE/Tyr19Phe and PsbE/Thr26Pro mutant cells did not recover to the same extent as that one observed for WT*3 cells. For the PsbE/His23Ala and PsbE/His23Met mutant cells, the oxygen evolution activity decreased to ≈ 40% of the initial one after 3 hours of high light illumination and remained stable. These results strongly suggest that the assembly of active PSII complexes which are unable to bind the Cytb_{559} haem (*i.e.* in the PsbA/His23Ala and PsbE/His23Met mutants) is slower than in the PsbE/Tyr19Phe and PsbE/Thr26Pro mutants and of course than in the WT*3 but that this assembly nevertheless occurs with a lower rate as evidenced by the lower steady state level of the activity under high light irradiation conditions. Since, the Cytb_{559} remained in the high potential form in the PsbE/Tyr19Phe mutant whereas it was converted into the low potential one in the PsbE/Thr26Pro mutant, at least in the purified thylakoid. The faster recovery observed in the PsbE/Thr26Pro than in PsbE/Tyr19Phe after high light illumination seems to indicate that there is not necessarily a correlation between the redox potential of the haem and the recovery rate.

4. Conclusions

- The presence of the apo-Cytb_{559} (*i.e.* with the PsbE and PsbF subunits alone) is sufficient to get the assembly of an active PSII with a high yield. The haem has no structural role provided that PsbE and PsbF are present.
- The steady state level of centers affected by high light illumination follows the order PsbE/His23Met ≈ PsbE/His23Ala > > PsbE/Tyr19Phe ≥ PsbE/Thr26Pro ≥ WT*3.
- The conversion of the high potential form into the low potential of the haem of Cytb_{559} and the lack of the haem do not accelerate the rate of photoinhibition which, in all cases, remains similar to that in the WT*3 cells.
- There is no correlation between the rate of photoinhibition and the redox potential of the haem.
- The rate of assembly of active PSII complexes lacking the haem (PsbE/His23Ala and PsbE/His23Met) is slower than in the Tyr19Phe and Thr26Pro mutants which, in turn, is slower that in the WT*3 cells.

Acknowledgements

We thank to Chizuko Azami, Yui Ozaki and Masato Nakamura (Ehime University) for technical assistance. This study was supported by JST-PRESTO program (4018 for M.S.) and Grant-in-Aid for scientific research from the Ministry of Education, Science, Sports, Culture and Technology (21612007 for M.S.). AB was supported in part by the French Infrastructure for Integrated Structural Biology (FRISBI) ANR-10-INSB-05-01 and the CEA/DSV "Bioénergie" program.

Appendix A. Supplementary data

Additional EPR data, growth rates of the strains and location of the amino acids in PsbE already mutated in the literature. Supplementary data associated with this article can be found, in the online version, at http://dx.doi.org/10.1016/j.bbabio.2014.11.009.

References

[1] Y. Umena, K. Kawakami, J.-R. Shen, N. Kamiya, Crystal structure of oxygen–evolving Photosystem II at a resolution of 1.9 Å, Nature 473 (2011) 55–60.
[2] F.H.M. Koua, Y. Umena, K. Kawakami, J.-R. Shen, Structure of Sr-substituted Photosystem II at 2.1 angstrom resolution and its implications in the mechanism of water oxidation, Proc. Natl. Acad. Sci. U. S. A. 110 (2013) 3389–3894.
[3] A. Guskov, J. Kern, A. Gabdulkhakov, M. Broser, A. Zouni, W. Saenger, Cyanobacterial Photosystem II at 2.9-angstrom resolution and the role of quinones, lipids, channels and chloride, Nat. Struct. Mol. Biol. 16 (2009) 334–342.
[4] B.A. Diner, F. Rappaport, Structure, dynamics, and energetic of the primary photochemistry of Photosystem II of oxygenic photosynthesis, Annu. Rev. Plant Biol. 53 (2002) 551–580.
[5] G. Renger, Light–induced oxidative water splitting in photosynthesis: energetics, kinetics, and mechanism, J. Photochem. Photobiol. B 104 (2011) 35–43.
[6] H. Dau, I. Zaharieva, M. Haumann, Recent developments in research on water oxidation by photosystem II, Curr. Opin. Chem. Biol. 16 (2012) 3–10.
[7] B. Kok, B. Forbush, M. McGloin, Cooperation of charges in photosynthetic O_2 evolution–I. A linear four step mechanism, Photochem. Photobiol. 11 (1970) 457–475.
[8] P. Joliot, B. Kok, Oxygen evolution in photosynthesis, in: Govindjee (Ed.), Bioenergetics of photosynthesis, Academic Press, New York, 1975, pp. 387–412.
[9] N. Cox, J. Messinger, Reflections on substrate water and dioxygen formation, Biochim. Biophys. Acta 1827 (2013) 1020–1030.
[10] J. Yano, V. Yachandra, Mn_4Ca cluster in photosynthesis: where and how water is oxidized to dioxygen, Chem. Rev. 114 (2014) 4175–4205.
[11] M.R.A. Blomberg, T. Borowski, F. Himo, R.Z. Liao, P.E.M. Siegbahn, Quantum chemical studies of mechanisms for metalloenzymes, Chem. Rev. 114 (2014) 3601–3658.
[12] H. Isobe, M. Shoji, S. Yamanaka, H. Mino, Y. Umena, K. Kawakami, N. Kamiya, J.-R. Shen, K. Yamaguchi, Generalized approximate spin projection calculations of effective exchange integrals of the CaMn4O5 cluster in the S-1 and S-3 states of the oxygen evolving complex of photosystem II, Phys. Chem. Chem. Phys. 16 (2014) 11911–11923.
[13] M. Roncel, D. Kirilovsky, F. Guerrero, A. Serrano, J.-M. Ortega, Photosynthetic cytochrome c550, Biochim. Biophys. Acta 1817 (2012) 1152–1163.
[14] R. Nagao, A. Moriguchi, T. Tomo, A. Niikura, S. Nakajima, T. Suzuki, A. Okumura, M. Iwai, J.-R. Shen, M. Ikeuchi, I. Enami, Binding and functional properties of five extrinsic proteins in oxygen-evolving photosystem II from a marine centric diatom, *Chaetoceros gracilis*, J. Biol. Chem. 285 (2010) 29191–29199.
[15] H. Andrews, Z.L. Li, A. Altuve-Blanco, M. Rivera, R.L. Burnap, Expression, mutagenesis, and characterization of recombinant low-potential cytochrome c(550) of photosystem II, Biochemistry 44 (2005) 6092–6100.
[16] M. Roncel, A. Boussac, J.L. Zurita, H. Bottin, M. Sugiura, D. Kirilovsky, J.-M. Ortega, Redox properties of the photosystem II cytochromes *b*559 and *c*550 in the cyanobacterium *Thermosynechococcus elongatus*, J. Biol. Inorg. Chem. 8 (2003) 206–216.
[17] C.A. Kerfeld, M.R. Sawaya, H. Bottin, K.T. Tran, M. Sugiura, D. Cascio, A. Desbois, T.O. Yeates, D. Kirilovsky, A. Boussac, Structural and EPR characterization of the soluble form of cytochrome c-550 and of the psbV2 gene product from the cyanobacterium *Thermosynechococcus elongatus*, Plant Cell Physiol. 44 (2003) 697–706.
[18] H. Ishikita, E.W. Knapp, Redox potential of cytochrome c550 in the cyanobacterium *Thermosynechococcus elongatus*, FEBS Lett. 579 (2005) 3190–3194.
[19] I. Enami, M. Iwai, A. Akiyama, T. Suzuki, A. Okumura, T. Katoh, O. Tada, H. Ohta, J.-R. Shen, Comparison of binding and functional properties of two extrinsic components, Cyt c550 and a 12 kDa protein, in cyanobacterial PSII with those in red algal PSII, Plant Cell Physiol. 44 (2003) 820–827.

[20] K.E. Shinopoulos, G.W. Brudvig, Cytochrome b559 and cyclic electron transfer within photosystem II, Biochim. Biophys. Acta 1817 (2012) 66–75.
[21] F. Guerrero, J.L. Zurita, M. Roncel, D. Kirilovsky, J.-M. Ortega, The role of the high potential form of the cytochrome b559: Study of *Thermosynechococcus elongatus* mutants, Biochim. Biophys. Acta 1837 (2014) 908–919.
[22] O.P. Kaminskaya, V.A. Shuvalov, Biphasic reduction of cytochrome b559 by plastoquinol in Photosystem II membrane fragments. Evidence for two types of cytochrome b559/plastoquinone redox equilibria, Biochim. Biophys. Acta 1827 (2013) 471–483.
[23] F. Muh, C. Glockner, J. Hellmich, A. Zouni, Light-induced quinone reduction in Photosystem II, Biochim. Biophys. Acta 1817 (2012) 44–65.
[24] N. Bondarava, C.M. Gross, M. Mubarakshina, J.R. Golecki, G.N. Johnson, A. Krieger-Liszkay, Putative function of cytochrome b559 as a plastoquinol oxidase, Physiol. Plant. 138 (2010) 463–473.
[25] P. Pospisil, I. Snyrychova, J. Kruk, K. Strzalka, J. Naus, Evidence that cytochrome b(559) is involved in superoxide production in photosystem II: effect of synthetic short-chain plastoquinones in a cytochrome b(559) tobacco mutant, Biochem. J. 397 (2006) 321–327.
[26] F. Morais, K. Kühn, D.H. Stewart, J. Barber, G.W. Brudvig, P. Nixon, Photosynthetic water oxidation in cytochrome b(559) mutants containing a disrupted haem-binding pocket, J. Biol. Chem. 276 (2001) 31986–31993.
[27] J.J. Ma, L.B. Li, Y.X. Jing, T.Y. Kuang, Mutation of residue Arginine(18) of cytochrome b(559) alpha-subunit and its effects on photosystem II activities in *Chlamydomonas reinhardtii*, J. Integr. Biol. 49 (2007) 1054–1061.
[28] J.J. Ma, L.B. Li, Y.X. Jing, T.Y. Kuang, Mutagenesis of Ser(24) of cytochrome b(559) alpha subunit affects PSII activities in *Chlamydomonas reinhardtii*, Chin. Sci. Bull. 52 (2007) 896–902.
[29] Y.F. Chiu, Y.H. Chen, M. Roncel, P.L. Dilbeck, J.Y. Huang, S.C. Ke, J.-M. Ortega, R.L. Burnap, H.-A. Chu, Spectroscopic and functional characterization of cyanobacterium *Synechocystis* PCC *6803* mutants on the cytoplasmic-side of cytochrome b559 in photosystem II, Biochim. Biophys. Acta 1827 (2013) 507–519.
[30] H.B. Pakrasi, P. Deciechi, J. Whitmarsh, Site directed mutagenesis of the heme axial ligands of cytochrome b559 affects the stability of the photosystem II complex, EMBO J. 10 (1991) 1619–1627.
[31] C.H. Hung, J.Y. Huang, Y.F. Chiu, H.-A. Chu, Site-directed mutagenesis on the heme axial-ligands of cytochrome b559 in photosystem II by using cyanobacteria *Synechocystis* PCC 6803, Biochim. Biophys. Acta 1767 (2007) 686–693.
[32] C.H. Hung, H.J. Hwang, Y.H. Chen, Y.F. Chiu, S.C. Ke, R.L. Burnap, H.-A. Chu, Spectroscopic and functional characterizations of cyanobacterium *Synechocystis* PCC 6803 mutants on and near the heme axial ligand of cytochrome b559 in photosystem II, J. Biol. Chem. 285 (2010) 5653–5663.
[33] Y.F. Chiu, W.C. Lin, C.M. Wu, Y.H. Chen, C.H. Hung, S.C. Ke, H.-A. Chu, Identification and characterization of a cytochrome b559 *Synechocystis* 6803 mutant spontaneously generated from DCMU-inhibited photoheterotrophical growth conditions, Biochim. Biophys. Acta 1787 (2009) 1179–1188.
[34] M.L. Hamilton, E. Franco, Z. deák, E. Schlodder, I. Vass, P.J. Nixon, Investigating the photoprotective role of Cytovhrome b-559 in Photosystem II in a mutant with altered ligation of the haem, Plant Cell Physiol. 55 (2014) 1276–1285.
[35] D.H. Stewart, G.W. Brudvig, Cytochrome b(559) of photosystem II, Biochim. Biophys. Acta 1367 (1998) 63–68.
[36] M. Roncel, J.-M. Ortega, M. Losada, Factors determining the special redox properties of photosynthetic cytochrome b559, Eur. J. Biochem. 268 (2001) 4961–4968.
[37] C. Berthomieu, A. Boussac, W. Mantele, J. Breton, E. Nabedrik, Molecular changes following oxido-reduction of cytochrome b559 characterized by FTIR spectroscopy: photooxidation in photosystem II and electrochemistry of isolated cytochrome b559 and iron protoporphyrin IX-bisimidazole model compounds, Biochemistry 31 (1992) 11460–11471.
[38] A.L. Yatsunyk, A. Dawson, M.D. Carducci, G.S. Nichol, F.A. Walker, Models of the cytochromes: Crystal structures and EPR spectral characterization of low-spin bis-imidazole complexes of (OETPP)FeIII having intermediate ligand plane dihedral angles, Inorg. Chem. 45 (2006) 5417–5428.
[39] M. Sugiura, A. Boussac, T. Noguchi, F. Rappaport, Influence of Histidine-198 of the D1 subunit on the properties of the primary electron donor, P680, of Photosystem II in *Thermosynechococcus elongatus*, Biochim. Biophys. Acta 1777 (2008) 331–342.
[40] M. Sugiura, Y. Inoue, Highly purified thermo-stable oxygen evolving Photosystem II core complex from the thermophilic cyanobacterium *Synechococcus elongatus* having His-tagged CP43, Plant Cell Physiol. 40 (1999) 1219–1231.
[41] W. Wohlleben, W. Arnold, L. Bissonette, A. Palletier, A. Tanguay, P.H. Roy, G.C. Ganboa, G.F. Barry, E. Aubert, J. Davies, S.A. Kagan, Small broad-host-range gentamycin resistance gene cassettes for site-specific insertion and deletion mutagenesis, Biotechniques 15 (1993) 831–834.
[42] M. Sugiura, C. Azami, K. Koyama, A.W. Rutherford, F. Rappaport, A. Boussac, Modification of the pheophytin redox potential in *Thermosynechococcus elongatus* Photosystem II with PsbA3 as D1, Biochim. Biophys. Acta 1837 (2014) 139–148.
[43] M. Sugiura, Y. Ozaki, M. Nakamura, N. Cox, F. Rappaport, A. Boussac, The D1–173 amino acid is a structural determinant of the critical interaction between D1-Tyr161 (TyrZ) and D1-His190 in Photosystem II, Biochim. Biophys. Acta 1837 (2014) 1922–1931.
[44] M. Ikeuchi, Y. Inoue, A new 4.8-kDa polypeptide intrinsic to the PS II reaction center, as revealed by modified SDS-PAGE with improved resolution of low-molecular-weight proteins, Plant Cell Physiol. 29 (1988) 1233–1239.
[45] M. Sugiura, E. Iwai, H. Hayashi, A. Boussac, Differences in the interactions between the subunits of Photosystem II dependant on D1 protein variants in the thermophilic cyanobacterium *Thermosynechococcus elongatus*, J. Biol. Chem. 285 (2010) 30008–30018.
[46] C. Fufezan, C.-X. Zhang, A. Krieger-Liszkay, A.W. Rutherford, Secondary quinone in photosystem II of *Thermosynechococcus elongatus*: Semiquinone-iron EPR signals and temperature dependence of electron transfer, Biochemistry 44 (2005) 12780–12789.